Does grain size influence hydrocarbons generation and mesoporosity during artificial thermal maturation of an organic-rich mudstone?

Amélie Cavelan, Mohammed Boussafir

Journal Pre-proof

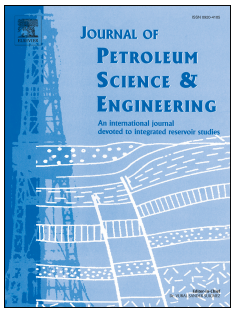

Does grain size influence hydrocarbons generation and mesoporosity during artificial thermal maturation of an organic-rich mudstone?

Amelie Cavelan, Mohammed Boussafir

PII: S0920-4105(21)01276-6

DOI: https://doi.org/10.1016/j.petrol.2021.109643

Reference: PETROL 109643

To appear in: *Journal of Petroleum Science and Engineering*

Received Date: 14 April 2021

Revised Date: 7 September 2021

Accepted Date: 7 October 2021

Please cite this article as: Cavelan, A., Boussafir, M., Does grain size influence hydrocarbons generation and mesoporosity during artificial thermal maturation of an organic-rich mudstone?, *Journal of Petroleum Science and Engineering* (2021), doi: https://doi.org/10.1016/j.petrol.2021.109643.

Author statement

Amelie Cavelan: Investigation - Original draft preparation- Redaction - Writing - Review & Editing. **Mohammed Boussafir**: Project administration - Conceptualization - Supervision- Review & Editing - Funding acquisition.

Does grain size influence hydrocarbons generation and mesoporosity during artificial thermal maturation of an organic-rich mudstone?

Amelie Cavelan [1, 2*], Mohammed Boussafir [1,3]

[1]Université d'Orléans, CNRS, BRGM, ISTO, UMR 7327, F-45071, Orléans, France

[2]Université de Lorraine, CNRS, LIEC, F-54000, Nancy, France

[3]Université de Tours, GeHCO, F-37200, Tours, France

*Corresponding author: amelie.cavelan@univ-lorraine.fr

Highlights

- The effect of sample grain sizes on laboratory thermal maturations is investigated.
- The use of small blocks, rocks fragments, and powder were compared
- The use of small blocks lowered the amount of the generated hydrocarbons.
- Lower pore sizes and volumes are measured for the small blocks
- The impact of the sample grain sizes differs between thermal maturation systems

Abstract

To assess how the grain size/rock fabric of laboratory-matured shale samples impact oil, gas production, and the formation of pores during laboratory thermal maturation, cores (4.5 mm*1 cm) of bulk rock, millimetric equidimensional rock fragments (3*3 mm), and fine grind powder (<200µm) were obtained from an organic-rich mudstone (Kimmeridge Clay Fm. "KCF", Yorkshire, UK) and artificially matured under anhydrous conditions. The composition of the organic matter (OM), porosity, and thermal maturity were characterized using nitrogen adsorption, Rock-Eval® VI pyrolysis, GC/TCD (Gas-Chromatography/Thermal Conductivity Detector), and GC/MS (Gas Chromatography/Mass Spectrometry). While only a few differences in geochemical composition and porosity exist between rock fragments and powders, a greater gap is observed with the cores. Probably due to lower surface contact between the organic components themselves and clay mineral surfaces (which can act as a

catalyst of oil and gas generation) less intense OM thermal degradation processes were observed for the cores. The use of cores rather than powder and fragments results in: (i) the production of lower extractible OM concentrations; (ii) lower amounts of gas (C_1-C_5 and CO_2); (iii) lower pore volumes and smaller pore sizes during maturation. This preliminary work highlights the importance of considering the fabric of the rock being artificially matured and shows that the use of cores with an intact rock fabric (e.g. cores), closer to natural conditions, could be more suitable when studying OM thermal degradation and porosity. In comparison with previous works, this also demonstrated that depending on the maturation system used (e.g. semi-confined, confined) the differences in the amount of hydrocarbons generated and porosity observed between powder and cores during maturation could differ significantly and find their origin in different processes.

Keywords: Artificial thermal maturation, rock fabric, mesoporosity, mudstone.

1. Introduction

A further understanding of the variation of the porosity of mudstones during maturation is necessary to predict the spots favorable for successful exploitation of shale oil and gas (Clarkson et al., 2013; Katz and Arango, 2018; Ross and Bustin, 2009). To better explain how OM composition and thermal maturity affect organic-rich mudstone porosity, laboratory thermal maturations were increasingly used these last years since they ensure to obtain rocks of different thermal maturity from the same initial immature sample (Cao et al., 2021; Cavelan et al., 2019a, 2020a; Chen and Xiao, 2014; Guo et al., 2017; Han et al., 2019; Ko et al., 2016, 2018; Song et al., 2020, 2021; Tan et al., 2021; T. Wang et al., 2021; Y. Wang et al., 2021; Xu et al., 2021). Initially used to calculate kinetic parameters, assess variations of the kerogen structure, mass balance, or quantify oil generation potential, this method significantly improved our knowledge about oil and gas generation mechanisms and hydrocarbon expulsion processes (Behar et al., 2010, 2008, 2003, 1997, 1992; Behar and Vandenbroucke, 1986; Hou et al., 2021; Landais et al., 1994; Lewan, 1997; Michels et al., 1994; Monthioux et al., 1985) and their relation with the formation of pores and the storage capacity of shale reservoirs (Cavelan et al., 2019a;

Chen and Xiao, 2014; Guo et al., 2017; Han et al., 2019; Ko et al., 2018; Song et al., 2020, 2021; T. Wang et al., 2021; Y. Wang et al., 2021; Xu et al., 2021). Today several conventional and MBE (material balance equation) models used to estimate the gas sorption capacity of kerogen at different thermal maturity are still partly based on the knowledge acquired during these experiments (Alafnan, 2021; Alafnan et al., 2020; Ambrose et al., 2012; Ungerer et al., 2015). However, the experimental conditions (open, semi-confined, confined, the chosen duration/temperature, hydrous/anhydrous conditions, rock fabric) chosen for these maturations is known to influence OM thermal degradation processes (Behar et al., 2003; Cavelan et al., 2020a; İnan, 2000; Landais et al., 1994; Michels et al., 1995; Monthioux, 1988; Shao et al., 2018; Song et al., 2021; Suárez-Ruiz et al., 1994). The mineral phase, and especially clay minerals, is known to act as a support medium of the OM and a catalyzer during its thermal transformations (Tannenbaum et al., 1986; Tannenbaum and Kaplan, 1985; Tissot and Welte, 2013). The relative distribution of OM and minerals in rocks, the size of the OM domains, and the degree of confinement of the system may influence oil and gas generation during burial (Michels et al., 1995, 1994; Suárez-Ruiz et al., 1994). In particular, during artificial maturation, OM diagenetic processes can be affected by the physical and morphological properties of the pyrolyzed sample (İnan, 2000; Shao et al., 2018; Song et al., 2021; Suárez-Ruiz et al., 1994). Probably due to better confinement achieved in core samples, these works observed different compositions and contents of hydrocarbons generated by the OM after the maturation of cores and powdered samples. In particular, they showed that the use of core samples may favor the expulsion of oil (Shao et al., 2018; Song et al., 2021). Considering the effect that the thermal degradation of OM can have on the development of mudstone porosity (Cavelan et al., 2020b; Chen and Xiao, 2014; Curtis et al., 2012; Fishman et al., 2012; Guo et al., 2017; Hackley and Cardott, 2016; Han et al., 2019; Katz and Arango, 2018; Klaver et al., 2015; Ko et al., 2018; Löhr et al., 2015; Loucks et al., 2009; Mastalerz et al., 2013; Milliken et al., 2014; Song et al., 2021, 2020; T. Wang et al., 2021; Y. Wang et al., 2021; Xu et al., 2021), we can suppose that the use of different rock particle sizes during artificial maturation may affect the thermal degradation of the OM, leading to different OM-hosted pore development. Indeed, Song et al. (2021) demonstrated that semi-closed pyrolysis of

type-II lacustrine mudstones gives different results in terms of hydrocarbon retention-expulsion mechanisms and pore development when performed on a powdered sample or cores.

Recent computation works for estimating the gas storage capacity of kerogen in shales are based on porosity parameters and in particular on Langmuir isotherms and Langmuir volumes which depend on the kerogen composition but also the porosity formed during maturation (Alafnan, 2021; Alafnan et al., 2020; Ambrose et al., 2012; He et al., 2019; Memon et al., 2020; Ungerer et al., 2015). The pore size distributions of shales may also largely influence gas-in-place calculation (Tolbert and Wu, 2015). Differences in specific surface area, pore-volume, or pore size distribution obtain between different thermal maturation conditions for the same maturity may, therefore, lead to differences in gas storage capacity and gas in place recovery estimations. Recent numerical works also demonstrated that the properties of the pore network such as the pore radius or the composition of the oils acquired during thermal maturation greatly influence the oil transport in shale micro-fractures and nanopores (Cui, 2019a). For example, the increase in the amount of generated asphaltenes may enhance the permeability of organic pores but reduce the permeability of inorganic pores and micro-fractures (Cui, 2019a), while the radius of pores and fractures controlled the permeability of shales that may impact pre-Darcy flow phenomena mechanisms (Cui, 2019b; Cui and Si, 2021). Therefore, an inaccurate estimation of these parameters (oil composition, oil quantity, pore sizes, etc.) linked to the choice of thermal maturation parameters could, for example, lead to an inaccurate estimation of the flow capacity/properties of the studied shale formation. However, to our knowledge, only Song et al. (2021) studied the impact of the rock fabric on the evolution of shale porosity during laboratory thermal maturation. This is insufficient to determine to which extent these results can be applied to all experimental thermal maturation works since they could depend on the maturation system used (semi-confined).

It is, therefore, necessary to better understand how these maturation conditions, which often differ from one study to another, affect the maturation of OM and the resulting porosity. To that end, cores, rock fragments, and powder of an immature mudstone from the Kimmeridge Clay Fm. (Yorkshire, UK) were artificially matured in autoclaves. The composition of the OM, thermal maturity, and

mesopore structure with increasing maturity were determined using nitrogen adsorption and bulk geochemical characterizations (Rock-Eval VI pyrolysis, GC-TCD (gas chromatography-thermal conductivity detector), and GC-MS (gas chromatography-mass spectrometry). The obtained data were compared with naturally matured rocks from the Vaca Muerta Fm. (Cavelan et al., 2020b, 2019b) to see which artificial sample series is closest to natural trends.

2. Methods

2.1. Sample

Three cores (4.5 mm*1 cm), rock fragments "RF" (3*3 mm), and powder "PO" (<250µm) were obtained from one immature mudstone from the Kimmeridge Clay Fm. (Yorkshire, UK). The properties of this sample are presented in Tab.1. For each sample type, 1g was firstly oven-dried at 105°C for 12 hours, placed separately in gold tubes before being introduced into high-pressure autoclaves in stainless steel. Each sample was then laboratory- matured under confined and anhydrous conditions at 325°C, 390°C, and 470°C for 72 hours (600 bars, external hydrostatic pressure) with the protocol defined by Cavelan et al. (2019b).

2.2. Rock-Eval

To determine the hydrogen index (HI, mg HC./g TOC), T_{max}, and total organic carbon (TOC, wt.%) contents of samples after maturation, 60 mg of each sample were crushed into powder and analyzed using new Rock-Eval 6® pyrolysis with the same procedure described in (Cavelan et al., 2019a). TOC was calculated from the integration of peaks S_1, S_2, S_3CO, S_3CO_2, S_4CO, and S_4CO_2 (see Espitalie et al., 1985). The HI represents the amount of pyrolyzed hydrocarbons and was calculated with the following equation (equation 1):

$$HI\ (mgHC/g\ TOC) = \frac{S2*100}{TOC} \quad (equation\ 1)$$

With S_2 the amount of hydrocarbons generated by the thermal cracking of the kerogen during the pyrolysis. The T_{max}-is often used as a maturity indicator and is derived from the T_{pic} which is the temperature of the peak oil production during pyrolysis (see Espitalie et al., 1985).

2.3. Gas chromatography

After maturation, 2 cm3 of gas were sampled with the protocol described in (Cavelan et al., 2019a) and injected in GC-TCD (Perkin Elmer® Clarus 580; Column Supelco® Carboxen 1010 Plot® Capillary: length: 30 m, film thickness: 0.15 µm, internal diameter 0.53 µm). Gas quantification was made using calibration curves and the areas of the peak of each gas on chromatograms. Then, 1g of all artificially matured samples was crushed into powdered and extracted in solvent (dichloromethane: methanol (1:1)) using ultrasonication. The extractible part of the OM (EOM) was then separated on a silica gel chromatography column and the fraction of aromatic (ARO), saturated (SAT), and polar hydrocarbons were then recovered separately by elution with different solvents using the protocol of Cavelan et al. (2020b). Asphaltene contents were obtained by the difference between the mass of the total extract and the mass of the recovered polar hydrocarbons, ARO and SAT. The compounds rich in Nitrogen, Sulfur, or Oxygen (NSO) represents the sum of the asphaltenes and polar hydrocarbons. The molecular composition of ARO and SAT were determined using a GC-MS Trace-GC Ultra (Column: Thermo Trace-Gold 5 MS, length 60 m, internal diameter 0.25 mm, film thickness 0.25 µm fitted by a mass spectrometer TSQ Quantum XLS. Compounds of interest in the ARO fraction were identified using retention times and mass spectra and quantified using their peak areas on ion-specific chromatograms. Squalane was the internal standard. Values of equivalent vitrinite reflectance (Rc, %) were then calculated using the methyldibenzothiophene ratios (MDTR), the dimethylphenanthrene ratios (DMPR), and the methylphenanthrene index (MPI-1) with the equation described by Radke et al. (1986) and Boreham et al. (1988). The mean of these three obtained Rc values is the mean Rc (%). Before and after maturation 60 mg of each sample were powdered and dried before being pyrolyzed using the Rock-Eval® VI method (Espitalié et al., 1985a, 1985b) to obtain : (i) the content of total organic carbon

(TOC, in weight % of the rock); (ii) the oil-prone quality of the OM expressed as a Hydrogen Index (HI, mg of HC per g of TOC).

2.4. Vintrinite reflectance

To confirm the calculated vitrinite reflectance values obtained from biomarker ratios (Rc), vitrinite reflectance (Rv) was measured on fragments and cores after thermal maturation. Measurements were carried on polished rock sections made from cores and fragments using the preparation and calibration protocol described in (Cavelan et al., 2020b). For each sample, each Rv value is the mean of 50 random measurements.

2.5. Nitrogen adsorption measurements

After maturation, the volume, the distribution of the pore sizes (PSD), and the BET surface area were measured using nitrogen adsorption (Quantachrome® NOVA 2200e). Before analysis, each sample was crushed to a particle size < 250 µm before being oven-dried for 12 hours (110°C). The samples were then outgassed for 24h (105°C) directly in the apparatus. The volume of pores accessible to nitrogen was determined using the liquid molar volume of nitrogen adsorbed at the relative pressure (P/Po) = 0.99 with the following equation (equation 2):

$$Pore\ volume\ (cm3/g) = \frac{amount\ of\ N2\ adsorbed\ at \frac{P}{P0}=0.99\ (cm3\ STP/g)}{647\ (N2\ liquid\ volume\ ratio\ at\ 77\ K)} \qquad \textit{(equation 2)}$$

PSDs were calculated on the adsorption isotherms using the method of Barrett et al. (1951) (often called the "BJH method"). BET surface areas were calculated using the Brunauer, Emmett, and Teller method applied to the adsorption isotherm (BET) between P/Po 0.03 and 0.33 (Brunauer et al., 1938). Each analysis of BET surface area was done with a minimum of 15 points. Analyses were done at the liquid nitrogen temperature (77K).

Preliminary results obtained by CO_2 (Quantachrome - Autosorb-1-MP-6) and N2 (Micromeritics® ASAP -2420) adsorption measurements using the Dubinin-Radushkevich model (DR), Dubunin-Astakhov between P/Po ranging from 0.0001 to 0.01 (adsorption isotherms), and the Horwath-Kawazoe

model between P/Po ranging from 1 to 0.35 showed that the studied samples are predominantly mesoporous. Microporosity (<2 nm) represents less than 8% of the pore volume and specific surface. Therefore, only mesoporosity (2-50 nm) and part of the macroporosity (> 50 nm) were investigated in this work.

Three replicates of thermal maturations were made from the same sample for each degree of maturity and each type of rock fabric. The presented results show the mean values and standard deviations obtained for these triplicates.

3. Results and discussion

3.1. Influence of particle size of the pyrolyzed rock on the amount and composition of generated hydrocarbons.

Variation of calculated (Rc) and measured vitrinite reflectance (Rv), HI, T_{max}, and concentrations of gas, SAT, NSO, and ARO shows that the three series of samples evolved from the oil to the gas window after heating from 325°C to 470°C (Tab.2, Fig.1). Whatever the rock fabric of the samples, the early stage of oil production was reached after heating at 325°C (Rc ~0.71%). After maturation at 390 and 470°C, the decrease of the HI, SAT, ARO, and NSO contents, the increase of C1-C5 hydrocarbons gases, and CO2 concentrations indicate the entry in the gas window (Tab.2, Fig.1). This is well substantiated by the Rc of 1.28% and 2.41% calculated after heating at 390°C and 470°C (Tab.2). Concerning the extracted OM composition, differences exist between series, especially between the cores and the two other sample types: RF and PO. The few differences observed between the PO and RF are less than 10% and are thus not significant. Even if special care has been taken to sample all series on one small and homogeneous rock, these differences can simply be explained by slight intern variations in the initial composition of the rock or by the slight differences attached to the OM extraction and analyses. These differences are therefore not sufficient to reveal any effect of the sample rock fabric on OM thermal degradation between these series. The experimental thermal maturation of powder and rock fragments gives thus comparable results and can be compared. Moreover, differences are greater

with the core series (Fig.1). The cores generated 25% less EOM (including NSO, ARO, and SAT concentrations) during the generation of oil (Rc ~0.71%). The relative proportions of ARO, SAT, and NSO are nevertheless similar between RF and PO series (~14%, 18%, and 68% respectively). A similar difference is observed during gas generation. While only a few negligible differences are observed between RF and PO during the condensate wet gas zone (Rc ~1.28%) and the dry gas zone (Rc ~2.41%), the cores generated ~ 30% fewer concentrations of C_1-C_5 and 50% to 84% fewer concentrations of CO_2 (Fig.1). All series of samples come from the same immature rock (a mudstone rich in OM) treated with the same experimental protocol, these differences are thus probably influenced by the fabric of the laboratory-matured samples. This supports previous results (İnan, 2000; Shao et al., 2018; Song et al., 2021; Suárez-Ruiz et al., 1994) and confirmes that the fabric of the rock affects the thermal maturation of the OM and thus the production of oil and gas. These results are in agreement with the observations of Shao et al. (2018), which shows that after thermal maturation under anhydrous conditions of shale samples from the Eagle Ford, the cores generated less C_1-C_5 and CO_2 concentrations than powdered samples. However, contrary to our study, Suárez-Ruiz et al. (1994) and Song et al. (2021) found that the cores had the highest oil yield than the powdered series during artificial thermal maturation. Based on previous works (Monthioux, 1988; Monthioux et al., 1985), Suárez-Ruiz et al. (1994) proposed that the increase of the grain size (e.g using cores) favored the retention of the pyrolysis effluents, allowing an increase in (i) the retention time of the compounds in the system; (ii) in the partial pressure of the effluents at the origin of the increase in oil yield during maturation. This assumption is also supported by Song et al. (2021). The thermal maturation of Suárez-Ruiz et al. (1994) and Song et al. (2021), was carried out using an open and semi-closed pyrolysis system respectively, in which the effluents are collected progressively during maturation. In the system of Suárez-Ruiz et al. (1994) no means of confinement is applied on samples, the different degree of confinement of the two sample series during oil generation created by the better ability of the cores to retain oil is therefore very important. In our case, all samples are matured in a confined environment inside sealed gold cells under inert gas and external hydrostatic pressure. This system has two advantages: (i) whatever the rock particle size, the

effluents are trapped in contact with the sample during maturation; (ii) although the means of confinement used in this system was not similar to the lithostatic pressure present in natural basins, it permits to reproduce for all series a certain degree of confinement required to accurately reproduce the thermal degradation of kerogen under laboratory conditions (Monthioux et al., 1985). According to these differences of artificial maturation conditions, we can therefore suggest that, in our case, variations in effluents' retention time or in the degree of confinement induced by the sample particle size that is being pyrolyzed are limited. The experimental device used by Song et al. (2021) reproduced both hydrostatic and lithostatic pressure conditions. The degree of confinement used is therefore also different from our experiments. This probably explains why we obtained so different results compared with these studies. However, this highlights the importance of the choice of laboratory thermal maturation conditions. Results from maturations under different conditions are not strictly comparable with each other or with natural samples. Results from laboratory maturation experiments should therefore be interpreted with caution. Concerning our experiments in anhydrous, closed, and confined conditions, the processes at the origin of the variations of oil and gas generation between our sample series are to be found elsewhere. We can suggest that the decrease in the sample particle size has: (i) increased the contact surface between the different OM components favoring the OM thermal degradation and increasing the yield of generated hydrocarbons; (ii) increased the contact surface between the OM and clay minerals. Previous works have indeed shown that the presence of Smectite or Illite (abundant in the Kimmeridge clay, Cavelan et al., 2019a) can act as catalysts for OM thermal degradation reactions (Huizinga et al., 1987; Tannenbaum et al., 1986; Tannenbaum and Kaplan, 1985). They showed that the strong adsorption capacities of these clay minerals and their ability to absorb and retain the heavy polar OM components favor the production of light, gaseous hydrocarbons, and the production of CO_2 during the cracking of OM. Increasing the surface contact between OM, all the effluents and the mineral surfaces have thus probably greatly favored the thermal degradation of the OM in the RF and the PO series compared to the cores during our laboratory simulations. This may explain the higher oil yield of the RF and the PO during oil generation but especially their higher C_1-C_5 and CO_2 concentrations during gas generation

(Fig.1). Shao et al. (2018)found comparable results for the Eagle Ford shales but suggested that the higher production of CO_2 was caused by an accelerated carbonates decomposition by the organic acids released by the OM thermal degradation. However, the upper Cretaceous Eagle Ford Shale is composed of carbonates with more than 80 wt% calcite (Ko et al., 2018; Shao et al., 2018). KCF samples contain less than 25% carbonates (Tab.1, Cavelan et al., 2019a), we can therefore conclude that the measured CO2 is also partly generated from the OM thermal degradation. Comparison with gas-matured Vaca Muerta rocks with similar TOC shows that cores give the closest EOM, ARO, and NSO concentrations during gas generation (Fig.1). The use of cores during artificial maturation may be more suitable to represent natural OM thermal degradation and that the decrease in the sample particle size may create an artificial enhancement of the OM thermal degradation process in the studied laboratory conditions.

3.2. Influence on rock mesoporosity

After heating at 325°C, the volume of pores and specific surface areas of the cores were low (0.26 cm3/100g and 2.0 m^2/g respectively) showing a poorly interconnected/low rock porosity. At this maturity stage the PO and the RF exhibit similar specific surface areas, volumes of pores, and PSDs (Fig.2A) which are mainly composed of ~50% of mesopores and macropores (Fig.2B). Then, with increasing maturity the specific surface area and the volume of pores increase in all series due to the appearance of pores with a diameter > 10 nm (Fig.2). This evolution in porosity may mark the formation of OM-hosted pores formed in response to oil and gas production (Bernard et al., 2012; Cao et al., 2021; Cavelan et al., 2020b, 2019a; Chalmers and Bustin, 2008; Curtis et al., 2012; Han et al., 2017; Ko et al., 2018, 2016; Loucks et al., 2009; T. Wang et al., 2021). While a few differences in PSDs, specific surface areas and pore volumes were observed between RF and PO series (Fig.2), for which similar quantity and composition of generated hydrocarbons were observed (Fig.1), significant differences in PSD, specific surface areas, pore volumes, EOM, SAR, ARO, NSO, and gas content exist between core series and the other series. During the production of gas, the pore volume of the cores is systematically lower with fewer pores larger than 10 nm (Fig.2A, B). On the contrary, the cores have larger specific surface areas due to the presence of smaller pores (<10 nm). Cores generated fewer hydrocarbons (liquid and

gaseous) during thermal maturation and therefore, have a lower oil and gas yield (Fig.1). The lower conversion of organic compounds in cores, related to the larger sample particle size, seems to lead to less or slower pore development. Thus, for similar thermal maturation conditions and maturity, porosity formed in cores is less developed, poorly connected (explaining why pores are inaccessible to nitrogen and not measurable in the oil window).

Comparison with naturally gas-matured Vaca Muerta samples showed once again, that the specific surface area and the PSD of core samples after maturation at 390°C and 470°C are the closest to the natural samples (Fig.2A, B). However, the pore volumes of Vaca Muerta samples are lower than for RF and PO and significantly higher than for the cores (Fig.2A). This may be related to the different mineralogy of the Vaca Muerta rocks (dominated by quartz) and KCF (dominated by clay, Cavelan et al., 2019a) which may influence the pore structure and the ability of the rock to preserve its porosity from deformation during maturation.

3.3 General implications

Considering these results and previous works (Shao et al., 2018; Song et al., 2021; Suárez-Ruiz et al., 1994), production, retention of hydrocarbons, and the composition of the oil and gas released by an organic-rich mudstone during artificial thermal maturation depend on the rock fabric of the pyrolyzed sample. This generates changes in the evolution of mesoporosity, specific surface areas, and pore volumes. While this confirms the close link existing between the OM thermal degradation reactions and porosity of OM-rich mudstones, it shows the importance of choosing the most appropriate thermal maturation parameters to simulate, as best as possible, the conditions of natural systems. As expected, in the light of our results natural samples seem better represented by core samples, which exhibit the most singular pore volumes and PSD after maturation and the closest features to naturally matured Vaca Muerta rocks. This suggests that confined anhydrous thermal maturation experiments previously carried out on powder and rock fragments may overestimate the amount of hydrocarbons generated and the associated pore volume that develops simultaneously. As observed between these three maturations

303 experiments and according to previous works, it must nevertheless be kept in mind that these results
304 show that the magnitude of these differences is influenced by the artificial maturation conditions (degree
305 and means of containment, hydrous pyrolysis…). Indeed, contrary to our observations in confined
306 environments, in semi-confined conditions, the use of powder seems to underestimate the yields of
307 generated oil and C4-C5 gases and to overestimate the yields of C1-C3 hydrocarbons (Song et al., 2021).
308 Predicting the differences between experimental maturation on powder, fragments or cores is, therefore,
309 not so easy. In recent years, a great number of works that aimed to better understand the physical-
310 chemical processes affecting the OM in source rocks, the porosity, and the storage capacity of
311 unconventional reservoirs were based on laboratory thermal maturation experiments (e.g. Cavelan et al.,
312 2020b, 2020c, 2019a; Gafurova et al., 2021; Guo et al., 2017; Ko et al., 2018, 2016; Song et al., 2020;
313 T. Wang et al., 2021; Wang et al., 2020; Wu et al., 2018; Xu et al., 2021; Yang et al., 2018). Many of
314 these papers compare their results with each other although they often used different thermal maturation
315 systems and sample rock fabrics. It is clear from these results that this could introduce biases into the
316 estimations of hydrocarbon production, permeability, gas storage capacity based on these results. For
317 example, the amount of NSO (including asphaltenes) generated during cores maturation is 35-50%
318 lower during the oil window than for powder and fragments (Fig.1). Recent numerical models showed
319 that the increase in the amount of generated asphaltenes may enhance the permeability of organic pores
320 but reduce the permeability of inorganic pores and micro-fractures of shales (Cui, 2019a). The organic
321 or inorganic pore permeability parameters of the same shale sample estimated by these mathematical
322 models could, therefore, vary greatly for the same thermal maturity depending on the sample rock fabric
323 used. Numerical models showed also that a change in pore sizes, distribution, connectivity, or shape will
324 influence the permeability of the rock and its flow properties (Cui, 2019a, 2019b). Our results show that
325 maturations on powder or fragments lead to different PSD and especially a lower number of micropores
326 than maturations on cores. Recent computations showed that the PSD, and in particular the number of
327 micropores in shales, has a strong influence on the gas in place calculation (Tolbert and Wu, 2015). In
328 our thermal maturation conditions, maturations of powder and fragments may, therefore, lead to an

underestimation of the amount of gas in place calculated by these models compared to maturations on cores. In general, models for estimating the gas sorption/storage capacity of kerogen or gas in place in shales use specific surface area or pore volume data based on Langmuir models (Alafnan et al., 2021; Alafnan et al., 2020; Ambrose et al., 2012; Hu et al., 2019; Memon et al., 2020; Tolbert and Wu 2015; Ungerer et al., 2015). The differences in pore volume and sizes observed between our thermal maturation experiments on cores, fragments, and powder, therefore, show that the choice of maturation parameters is crucial to ensure consistent estimates of shale reservoirs' properties. Most recent studies aimed to improve their models for predicting the quality and recoverability of the studied reservoirs using thermal maturation. It is therefore urgent to consider the effect of the experimental conditions used for thermal maturations to move towards standardization of thermal maturation techniques for a better and reliable understanding of the factors affecting hydrocarbon production, yields, and shale porosity (and without introducing biases due to differences in experimental maturation conditions between studies).

4. Conclusions

Laboratory thermal maturations of cores, fragments, and powder from the same organic-rich Kimmeridge Clay mudstone were compared. The results reveal that only a few differences of OM geochemical composition and porosity exist between rock fragments and powder series for each stage of maturation while cores give different results. Probably due to the lower surface contact between the organic components themselves and clay mineral surfaces (which can act as a catalyst for oil and gas generation) in cores, the OM undergoes a less effective thermal degradation characterized by (i) the production of lower SAT, ARO and NSO concentrations during oil production; (ii) lower C_1-C_5 and CO_2 concentrations during gas generation. This is marked by lower/less interconnected pore volume and smaller pores in the cores. This work shows that the amount of oil and gas and porosity may be influenced by the sample particle size used for laboratory thermal maturation. These experiments highlight, therefore, the importance of considering the particle size of the rock that is being pyrolyzed when studying OM thermal degradation and its relation with mudstones porosity. However, if these maturations in a confined and anhydrous environment on powder and fragments overestimate the

quantity of oil and C_1-C_5 hydrocarbons generated during thermal maturations compared to samples with an intact fabric (i.e cores), the opposite tendency has been observed in previous maturations in semi-confined environments. The comparison with equivalent (in terms of TOC and OM composition) naturally gas-mature rocks from the Vaca Muerta Fm. show that cores give the closest results to natural trends and appear thus, more suitable for artificial thermal maturation. Indeed, the use of powder or fragments leads to significant variations in composition and amount of generated hydrocarbons, specific surface areas, PSD, and pore volumes which can lead to a significant deviation from natural trends.

Acknowledgments

The authors would like to thank Mrs. Rachel Boscardin, Dr. Rémi Champallier, and Mrs. Nathalie Lottier for their support during experiments. Many thanks for the professional help of anonymous reviewers and editors which have greatly improved the quality of this work. This work was partly funded by the French National Research Agency (ANR) as part of the program "Investments d'Avenir" LabEx VOLTAIRE, 10-LABX-0100. This work was supported by the French council of the region Centre-Val de Loire.

References

Alafnan, S., 2021. Petrophysics of Kerogens Based on Realistic Structures. ACS Omega 6, 9549–9558.

Alafnan, S., Solling, T., Mahmoud, M., 2020. Effect of Kerogen Thermal Maturity on Methane Adsorption Capacity: A Molecular Modeling Approach. Molecules 25, 3764. https://doi.org/10.3390/molecules25163764

Ambrose, R.J., Hartman, R.C., Diaz-Campos, M., Akkutlu, I.Y., Sondergeld, C.H., 2012. Shale gas-in-place calculations part I: new pore-scale considerations. Spe J. 17, 219–229. https://doi.org/10.2118/131772-PA

Barrett, E.P., Joyner, L.G., Halenda, P.P., 1951. The determination of pore volume and area distributions in porous substances. I. Computations from nitrogen isotherms. J. Am. Chem. Soc. 73, 373–380. https://doi.org/10.1021/ja01145a126

Behar, F., Kressmann, S., Rudkiewicz, J.L., Vandenbroucke, M., 1992. Experimental simulation in a confined system and kinetic modelling of kerogen and oil cracking. Org. Geochem. 19, 173–189. https://doi.org/10.1016/0146-6380(92)90035-V

Behar, F., Lewan, M.D., Lorant, F., Vandenbroucke, M., 2003. Comparison of artificial maturation of lignite in hydrous and nonhydrous conditions. Org. Geochem. 34, 575–600. https://doi.org/10.1016/S0146-6380(02)00241-3

Behar, F., Lorant, F., Lewan, M., 2008. Role of NSO compounds during primary cracking of a Type II kerogen and a Type III lignite. Org. Geochem. 39, 1–22. https://doi.org/10.1016/j.orggeochem.2007.10.007

Behar, F., Roy, S., Jarvie, D., 2010. Artificial maturation of a Type I kerogen in closed system: Mass balance and kinetic modelling. Org. Geochem. 41, 1235–1247. https://doi.org/10.1016/j.orggeochem.2010.08.005

Behar, F., Vandenbroucke, M., 1986. Représentation chimique de la structure des kérogènes et des asphaltènes en fonction de leur origine et de leur degré d'évolution. Rev. Inst. Fr. Pétrole 41, 173–188. https://doi.org/10.2516/ogst:1986010

Behar, F., Vandenbroucke, M., Tang, Y., Marquis, F., Espitalie, J., 1997. Thermal cracking of kerogen in open and closed systems: determination of kinetic parameters and stoichiometric coefficients for oil and gas generation. Org. Geochem. 26, 321–339. https://doi.org/10.1016/S0146-6380(97)00014-4

Bernard, S., Horsfield, B., Schulz, H.-M., Wirth, R., Schreiber, A., Sherwood, N., 2012. Geochemical evolution of organic-rich shales with increasing maturity: A STXM and TEM study of the Posidonia Shale (Lower Toarcian, northern Germany). Mar. Pet. Geol. 31, 70–89. https://doi.org/10.1016/j.marpetgeo.2011.05.010

Boreham, C.J., Crick, I.H., Powell, T.G., 1988. Alternative calibration of the Methylphenanthrene Index against vitrinite reflectance: Application to maturity measurements on oils and sediments. Org. Geochem. 12, 289–294. https://doi.org/10.1016/0146-6380(88)90266-5

Brunauer, S., Emmett, P.H., Teller, E., 1938. Adsorption of gases in multimolecular layers. J. Am. Chem. Soc. 60, 309–319. https://doi.org/10.1021/ja01269a023

Cao, T., Deng, M., Cao, Q., Huang, Y., Yu, Y., Cao, X., 2021. Pore formation and evolution of organic-rich shale during the entire hydrocarbon generation process: Examination of artificially and naturally matured samples. J. Nat. Gas Sci. Eng. 104020. https://doi.org/10.1016/j.jngse.2021.104020

Cavelan, A., Boussafir, M., Le Milbeau, C., Delpeux, S., Laggoun-Défarge, F., 2020a. Influence of experimental temperature and duration of laboratory confined thermal maturation experiments on the evolution of the porosity of organic-rich source rocks. Mar. Pet. Geol. 122, 104667. https://doi.org/10.1016/j.marpetgeo.2020.104667

Cavelan, A., Boussafir, M., Le Milbeau, C., Laggoun-Défarge, F., 2020b. Impact of Oil-Prone Sedimentary Organic Matter Quality and Hydrocarbon Generation on Source Rock Porosity: Artificial Thermal Maturation Approach. ACS Omega. https://doi.org/10.1021/acsomega.0c01432

Cavelan, A., Boussafir, M., Le Milbeau, C., Rozenbaum, O., Laggoun-Défarge, F., 2019a. Effect of organic matter composition on source rock porosity during confined anhydrous thermal maturation: Example of Kimmeridge-clay mudstones. Int. J. Coal Geol. 212, 103236. https://doi.org/10.1016/j.coal.2019.103236

Cavelan, A., Boussafir, M., Mathieu, N., Laggoun-Défarge, F., 2020c. Impact of thermal maturity on the concomitant evolution of the ultrafine structure and porosity of marine mudstones organic matter; contributions of electronic imaging and new spectroscopic investigations. Int. J. Coal Geol. 103622. https://doi.org/10.1016/j.coal.2020.103622

Cavelan, A., Boussafir, M., Rozenbaum, O., Laggoun-Défarge, F., 2019b. Organic petrography and pore structure characterization of low-mature and gas-mature marine organic-rich mudstones: Insights into porosity controls in gas shale systems. Mar. Pet. Geol. 103, 331–350. https://doi.org/10.1016/j.marpetgeo.2019.02.027

Chalmers, G.R., Bustin, R.M., 2008. Lower Cretaceous gas shales in northeastern British Columbia, Part I: geological controls on methane sorption capacity. Bull. Can. Pet. Geol. 56, 1–21. https://doi.org/10.2113/gscpgbull.56.1.1

Chen, J., Xiao, X., 2014. Evolution of nanoporosity in organic-rich shales during thermal maturation. Fuel 129, 173–181. https://doi.org/10.1016/j.fuel.2014.03.058

Clarkson, C.R., Solano, N., Bustin, R.M., Bustin, A.M.M., Chalmers, G.R.L., He, L., Melnichenko, Y.B., Radliński, A.P., Blach, T.P., 2013. Pore structure characterization of North American shale gas reservoirs using USANS/SANS, gas adsorption, and mercury intrusion. Fuel 103, 606–616. https://doi.org/10.1016/j.fuel.2012.06.119

Cui, J., 2019a. Oil transport in shale nanopores and micro-fractures: Modeling and analysis. J. Pet. Sci. Eng. 178, 640–648. https://doi.org/10.1016/j.petrol.2019.03.088

Cui, J., 2019b. Pre-Darcy flow in shales: Effects of the rate-dependent slip. J. Pet. Sci. Eng. 183, 106393. https://doi.org/10.1016/j.petrol.2019.106393

Cui, J., Si, G., 2021. Equivalent anisotropic permeability of shale rocks: Effect of micro-fractures. J. Pet. Sci. Eng. 207, 109085. https://doi.org/10.1016/j.petrol.2021.109085

Curtis, M.E., Cardott, B.J., Sondergeld, C.H., Rai, C.S., 2012. Development of organic porosity in the Woodford Shale with increasing thermal maturity. Int. J. Coal Geol. 103, 26–31. https://doi.org/10.1016/j.coal.2012.08.004

Espitalié, J., Deroo, G., Marquis, F., 1985a. La pyrolyse Rock-Eval et ses applications. Première partie. Rev. Inst. Fr. Pétrole 40, 563–579. https://doi.org/10.2516/ogst:1985035

Espitalié, J., Deroo, G., Marquis, F., 1985b. La pyrolyse Rock-Eval et ses applications. Deuxième partie. Rev. Inst. Fr. Pétrole 40, 755–784. https://doi.org/10.2516/ogst:1985045

Fishman, N.S., Hackley, P.C., Lowers, H.A., Hill, R.J., Egenhoff, S.O., Eberl, D.D., Blum, A.E., 2012. The nature of porosity in organic-rich mudstones of the Upper Jurassic Kimmeridge Clay Formation, North Sea, offshore United Kingdom. Int. J. Coal Geol. 103, 32–50.

Gafurova, D., Kalmykov, A., Korost, D., Kalmykov, G., 2021. Macropores generation in the domanic formation shales: Insights from pyrolysis experiments. Fuel 289, 119933. https://doi.org/10.1016/j.fuel.2020.119933

Guo, H., Jia, W., Zeng, J., He, R., 2017. Evolution of organic matter and nanometer-scale pores in an artificially matured shale undergoing two distinct types of pyrolysis: A study of the Yanchang Shale with Type II kerogen. Org. Geochem. 105, 56–66. https://doi.org/10.1016/j.orggeochem.2017.01.004

Hackley, P.C., Cardott, B.J., 2016. Application of organic petrography in North American shale petroleum systems: A review. Int. J. Coal Geol. 163, 8–51.

Han, H., Guo, C., Zhong, N., Pang, P., Chen, S., Lu, J.-G., Gao, Y., 2019. Pore structure evolution of lacustrine shales containing type I organic matter from the upper cretaceous Qingshankou formation, Songliao Basin, China: A study of artificial samples from hydrous pyrolysis experiments. Mar. Pet. Geol. 104, 375–388. https://doi.org/10.1016/j.marpetgeo.2019.04.001

Han, Y., Horsfield, B., Wirth, R., Mahlstedt, N., Bernard, S., 2017. Oil retention and porosity evolution in organic-rich shales. AAPG Bull. 101, 807–827. https://doi.org/10.1306/09221616069

He, L., Mei, H., Hu, X., Dejam, M., Kou, Z., Zhang, M., 2019. Advanced flowing material balance to determine original gas in place of shale gas considering adsorption hysteresis. SPE Reserv. Eval. Eng. 22, 1282–1292. https://doi.org/10.2118/195581-PA

Hou, L., Ma, W., Luo, X., Liu, J., Liu, S., Zhao, Z., 2021. Hydrocarbon generation-retention-expulsion mechanism and shale oil producibility of the permian lucaogou shale in the Junggar Basin as simulated by semi-open pyrolysis experiments. Mar. Pet. Geol. 125, 104880. https://doi.org/10.1016/j.marpetgeo.2020.104880

Huizinga, B.J., Tannenbaum, E., Kaplan, I.R., 1987. The role of minerals in the thermal alteration of organic matter—III. Generation of bitumen in laboratory experiments. Org. Geochem. 11, 591–604. https://doi.org/10.1016/0146-6380(87)90012-X

İnan, S., 2000. Gaseous hydrocarbons generated during pyrolysis of petroleum source rocks using unconventional grain-size: implications for natural gas composition. Org. Geochem. 31, 1409–1418. https://doi.org/10.1016/S0146-6380(00)00070-X

Katz, B.J., Arango, I., 2018. Organic porosity: a geochemist's view of the current state of understanding. Org. Geochem. 123, 1–16. https://doi.org/10.1016/j.orggeochem.2018.05.015

Klaver, J., Desbois, G., Littke, R., Urai, J.L., 2015. BIB-SEM characterization of pore space morphology and distribution in postmature to overmature samples from the Haynesville and Bossier Shales. Mar. Pet. Geol. 59, 451–466.

Ko, L.T., Loucks, R.G., Zhang, T., Ruppel, S.C., Shao, D., 2016. Pore and pore network evolution of Upper Cretaceous Boquillas (Eagle Ford–equivalent) mudrocks: Results from gold tube pyrolysis experiments. AAPG Bull. 100, 1693–1722. https://doi.org/10.1306/04151615092

Ko, L.T., Ruppel, S.C., Loucks, R.G., Hackley, P.C., Zhang, T., Shao, D., 2018. Pore-types and pore-network evolution in Upper Devonian-Lower Mississippian Woodford and Mississippian Barnett mudstones: Insights from laboratory thermal maturation and organic petrology. Int. J. Coal Geol. 190, 3–28. https://doi.org/10.1016/j.coal.2017.10.001

Landais, P., Michels, R., Elie, M., 1994. Are time and temperature the only constraints to the simulation of organic matter maturation? Org. Geochem. 22, 617–630. https://doi.org/10.1016/0146-6380(94)90128-7

Lewan, M.D., 1997. Experiments on the role of water in petroleum formation. Geochim. Cosmochim. Acta 61, 3691–3723. https://doi.org/10.1016/S0016-7037(97)00176-2

Löhr, S.C., Baruch, E.T., Hall, P.A., Kennedy, M.J., 2015. Is organic pore development in gas shales influenced by the primary porosity and structure of thermally immature organic matter? Org. Geochem. 87, 119–132.

Loucks, R.G., Reed, R.M., Ruppel, S.C., Jarvie, D.M., 2009. Morphology, genesis, and distribution of nanometer-scale pores in siliceous mudstones of the Mississippian Barnett Shale. J. Sediment. Res. 79, 848–861. https://doi.org/10.2110/jsr.2009.092

Mastalerz, M., Schimmelmann, A., Drobniak, A., Chen, Y., 2013. Porosity of Devonian and Mississippian New Albany Shale across a maturation gradient: Insights from organic petrology, gas adsorption, and mercury intrusionGeohorizon. AAPG Bull. 97, 1621–1643.

Memon, A., Li, A., Muther, T., Ren, X., 2020. An experimental study of gas sorption, adsorbed, and sorbed porosity, and their impact on shale gas-in-place calculations. J. Porous Media 23. https://10.1615/JPorMedia.2020033387

Michels, R., Landais, P., Philp, R.P., Torkelson, B.E., 1994. Effects of pressure on organic matter maturation during confined pyrolysis of Woodford kerogen. Energy Fuels 8, 741–754. https://doi.org/10.1021/ef00045a031

Michels, R., Landais, P., Torkelson, B.E., Philp, R.P., 1995. Effects of effluents and water pressure on oil generation during confined pyrolysis and high-pressure hydrous pyrolysis. Geochim. Cosmochim. Acta 59, 1589–1604. https://doi.org/10.1016/0016-7037(95)00065-8

Milliken, K.L., Ko, L.T., Pommer, M., Marsaglia, K.M., 2014. SEM petrography of eastern Mediterranean sapropels: Analogue data for assessing organic matter in oil and gas shales. J. Sediment. Res. 84, 961–974.

Monthioux, M., 1988. Expected mechanisms in nature and in confined-system pyrolysis. Fuel 67, 843–847. https://doi.org/10.1016/0016-2361(88)90160-3

Monthioux, M., Landais, P., Monin, J.-C., 1985. Comparison between natural and artificial maturation series of humic coals from the Mahakam delta, Indonesia. Org. Geochem. 8, 275–292. https://doi.org/10.1016/0146-6380(85)90006-3

Radke, M., 1988. Application of aromatic compounds as maturity indicators in source rocks and crude oils. Mar. Pet. Geol. 5, 224–236. https://doi.org/10.1016/0264-8172(88)90003-7

Radke, M., Welte, D.H., Willsch, H., 1986. Maturity parameters based on aromatic hydrocarbons: Influence of the organic matter type. Org. Geochem. 10, 51–63. https://doi.org/10.1016/0146-6380(86)90008-2

Ross, D.J., Bustin, R.M., 2009. The importance of shale composition and pore structure upon gas storage potential of shale gas reservoirs. Mar. Pet. Geol. 26, 916–927. https://doi.org/10.1016/j.marpetgeo.2008.06.004

Shao, D., Ellis, G.S., Li, Y., Zhang, T., 2018. Experimental investigation of the role of rock fabric in gas generation and expulsion during thermal maturation: Anhydrous closed-system pyrolysis of a bitumen-rich Eagle Ford Shale. Org. Geochem. 119, 22–35. https://doi.org/10.1016/j.orggeochem.2018.01.012

Song, D., Wang, X., Tuo, J., Wu, C., Zhang, M., Su, L., He, W., 2021. A comprehensive study on the impacts of rock fabric on hydrocarbon generation and pore structure evolution of shale under semi-confined condition. Mar. Pet. Geol. 124, 104830. https://doi.org/10.1016/j.marpetgeo.2020.104830

Song, D., Wang, X., Wu, C., Meng, S., Zhang, M., Li, H., Jiao, H., Liu, X., Jin, X., Tuo, J., 2020. Petroleum Generation, Retention, and Expulsion in Lacustrine Shales Using an Artificial Thermal Maturation Approach: Implications for the In-Situ Conversion of Shale Oil. Energy Fuels. https://doi.org/10.1021/acs.energyfuels.0c03045

Suárez-Ruiz, I., Martinez, L., Bertrand, P., Prado, J.G., Disnar, J.-R., 1994. Influence of rock particle size on the artificial thermal evolution of kerogen. A petrographic and geochemical study. Int. J. Coal Geol. 25, 47–64. https://doi.org/10.1016/0166-5162(94)90004-3

Tan, J., Hu, R., Luo, W., Ma, Z., He, G., 2021. Pore Evolution of Lacustrine Organic-Rich Shales: Insights from Thermal Simulation Experiments. Energy Fuels 35, 3079–3094. https://doi.org/10.1021/acs.energyfuels.0c03828

Tannenbaum, E., Huizinga, B.J., Kaplan, I.R., 1986. Role of minerals in thermal alteration of organic matter—II: A material balance. AAPG Bull. 70, 1156–1165. https://doi.org/10.1306/94886A92-1704-11D7-8645000102C1865D

Tannenbaum, E., Kaplan, I.R., 1985. Role of minerals in the thermal alteration of organic matter—I: Generation of gases and condensates under dry condition. Geochim. Cosmochim. Acta 49, 2589–2604. https://doi.org/10.1016/0016-7037(85)90128-0

Tissot, B.P., Welte, D.H., 2013. Petroleum formation and occurrence. Springer Science & Business Media.

Tolbert, B.T., Wu, X., 2015. Quantifying Pore Size Distribution Effect on Gas in Place and Recovery Using SLD-PR EOS for Multiple-Components Shale Gas Reservoir. Presented at the SPE Asia

564 Pacific Unconventional Resources Conference and Exhibition, OnePetro.
565 https://doi.org/10.2118/176992-MS

566 Ungerer, P., Collell, J., Yiannourakou, M., 2015. Molecular Modeling of the Volumetric and
567 Thermodynamic Properties of Kerogen: Influence of Organic Type and Maturity. Energy Fuels
568 29, 91–105. https://doi.org/10.1021/ef502154k

569 Wang, T., Wang, Q., Lu, H., Zhan, X., 2021. Understanding pore evolution in a lacustrine calcareous
570 shale reservoir in the oil window by pyrolyzing artificial samples in a semi-closed system. J.
571 Pet. Sci. Eng. 200, 108230. https://doi.org/10.1016/j.petrol.2020.108230

572 Wang, Y., Liu, L., Cheng, H., 2021. Gas Adsorption Characterization of Pore Structure of Organic-rich
573 Shale: Insights into Contribution of Organic Matter to Shale Pore Network. Nat. Resour. Res.
574 30, 2377–2395. https://doi.org/10.1007/s11053-021-09817-5

575 Wang, Y., Liu, L., Hu, Q., Hao, L., Wang, X., Sheng, Y., 2020. Nanoscale pore network evolution of
576 Xiamaling Marine Shale during organic matter maturation by hydrous pyrolysis. Energy Fuels
577 34, 1548–1563. https://doi.org/10.1021/acs.energyfuels.9b03686

578 Wu, L., Geng, A., Wang, P., 2018. Oil expulsion in marine shale and its influence on the evolution of
579 nanopores during semi-closed pyrolysis. Int. J. Coal Geol. 191, 125–134.
580 https://doi.org/10.1016/j.coal.2018.04.001

581 Xu, L., Yang, K., Zhang, L., Liu, L., Jiang, Z., Li, X., 2021. Organic-induced nanoscale pore structure
582 and adsorption capacity variability during artificial thermal maturation: Pyrolysis study of the
583 Mesoproterozoic Xiamaling marine shale from Zhangjiakou, Hebei, China. J. Pet. Sci. Eng. 202,
584 108502. https://doi.org/10.1016/j.petrol.2021.108502

585 Yang, S., Chen, G., Lv, C., Li, C., Yin, N., Yang, F., Xue, L., 2018. Evolution of nanopore structure in
586 lacustrine organic-rich shales during thermal maturation from hydrous pyrolysis, Minhe Basin,
587 Northwest China. Energy Explor. Exploit. 36, 265–281.
588 https://doi.org/10.1177%2F0144598717723647

589

590

591 **Tables**

592

593 Tab.1. Location and main properties of the studied sample.

Location					
Basin	Formation		Well		Depth (m)
Cleaveland Basin (UK)	Kimmeridge Clay		Ebberston87		69.98
Mineralogy (wt.%)[a]					
Quartz	Calcite	Gypsum	Clay	Pyrite	Albite
8.7	17.6	0.8	53.6	5.7	3.0
Rock Eval parameters[b]					
TOC (wt.%)	S1 (mgHC/g rock)	S2 (mgHC/g rock)	IH (mgHC/g TOC)		IO (mg CO2/g TOC)
10.3	0.2	57.4	557		14
Vitrinite reflectance (%)[b]					
0.43					

594 [a] (Cavelan et al., 2019b);[b] (Cavelan et al., 2019a)

595

596 Tab.2. Mean calculated vitrinite reflectance (Rc), measured vitrinite reflectance (Rv), TOC, and Hydrogen index (HI) after maturation.

		MDTR[2]	R_{MDTR} (%)	Std Dev.	MPI-1[3]	R_{MPI} (%)	Std Dev	DMPR[2]	R_{DMPR} (%)	Std Dev	Mean R_c (%)	Std Dev.	HI (mg/g TOC)	TOC (wt.%)	Tmax	Rv (%)	Std Dev.
Powder Fragments	325°C	1.5	0.68	0.02	0.81	0.79	0.04	0.28	0.76	0.01	0.74	0.06	481	10.2	442		
		1.29	0.65	0.03	0.56	0.61	0.02	0.29	0.78	0.03	0.68	0.09	478	10.2	442	0.70	0.04
Cores		1.29	0.65	0.01	0.70	0.71	0.03	0.28	0.76	0.02	0.71	0.05	476	10.1	443	0.68	0.03
	Mean	1.36	0.66		0.69	0.70		0.28	0.77		0.71		478	10.2		0.69	
Powder Fragments	390°C	6.25	1.29	0.05	1.59	1.33	0.06	0.69	1.28	0.04	1.3	0.03	146	7.2	470		
		5.99	1.19	0.07	1.36	1.17	0.04	0.87	1.42	0.04	1.26	0.14	151	6.7	un	1.32	0.05
Cores		5.94	1.17	0.05	1.48	1.26	0.05	0.85	1.41	0.06	1.28	0.12	104	8.2	489	1.38	0.04
	Mean	6.06	1.22		1.48	1.25		0.80	1.37		1.28		134	7.4		1.35	
Powder Fragments	470°C	8.21	2.62	0.10	0.72	2.6	0.13	5.6	2.5	0.13	2.58	0.07	7	7.0	un		
		7.75	2.20	0.15	0.38	2.79	0.15	2.21	1.96	0.10	2.32	0.43	7	7.6	un	2.34	0.08
Cores		7.90	2.33	0.10	0.3	2.84	0.16	1.77	1.83	0.14	2.33	0.5	15	8.3	un	2.13	0.10
	Mean	7.96	2.38		0.47	2.74		3.19	2.10		2.41		10	7.6		2.24	

597 [1]*MDTR: ratio of methyldibenzothiophene* (Radke et al., 1986)***;*** R_{MDTR} *(%) calculated with the equation of Radke, (1988).* [2]*DMPR: ratio of dimethylphenanthrene*

598 (Radke et al., 1986)*.* R_{DMPR} *was calculated with the equation of Radke (1988).* [3]*MPI-1: index of methylphenanthrene* (Radke et al., 1986). R_{MPI-1} *calculated with*

599 *the equation of Boreham et al. (1988) for* R_v *between 0.3-1.7% and* R_v *> 1.7%.*

600

601 **Figures**

602

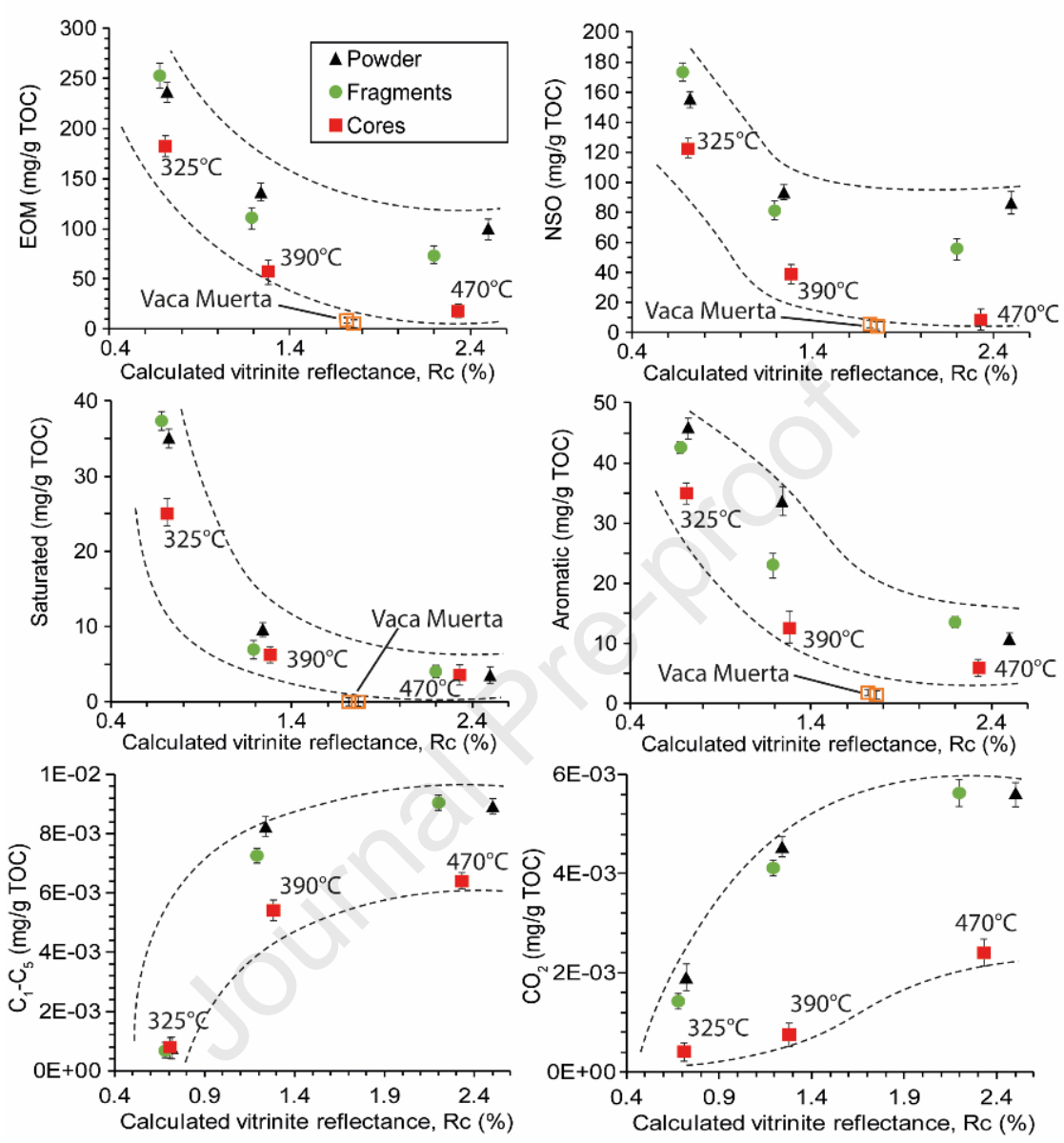

603

604 Fig.1. Evolution of Extractable Organic Matter (EOM), NSO, saturated, aromatic, C_1-C_5 hydrocarbon
605 gases, and CO_2 concentrations as a function of the sample type during maturation. Comparison with
606 Vaca Muerta samples (similar composition of the OM with the Kimmeridge Clay, Vitrinite reflectance
607 = 1.65 and 1.69%, TOC = 5.0 and 6.7 wt.%, HI = 43 and 19 mg/g HC, Cavelan et al., 2019a).

608

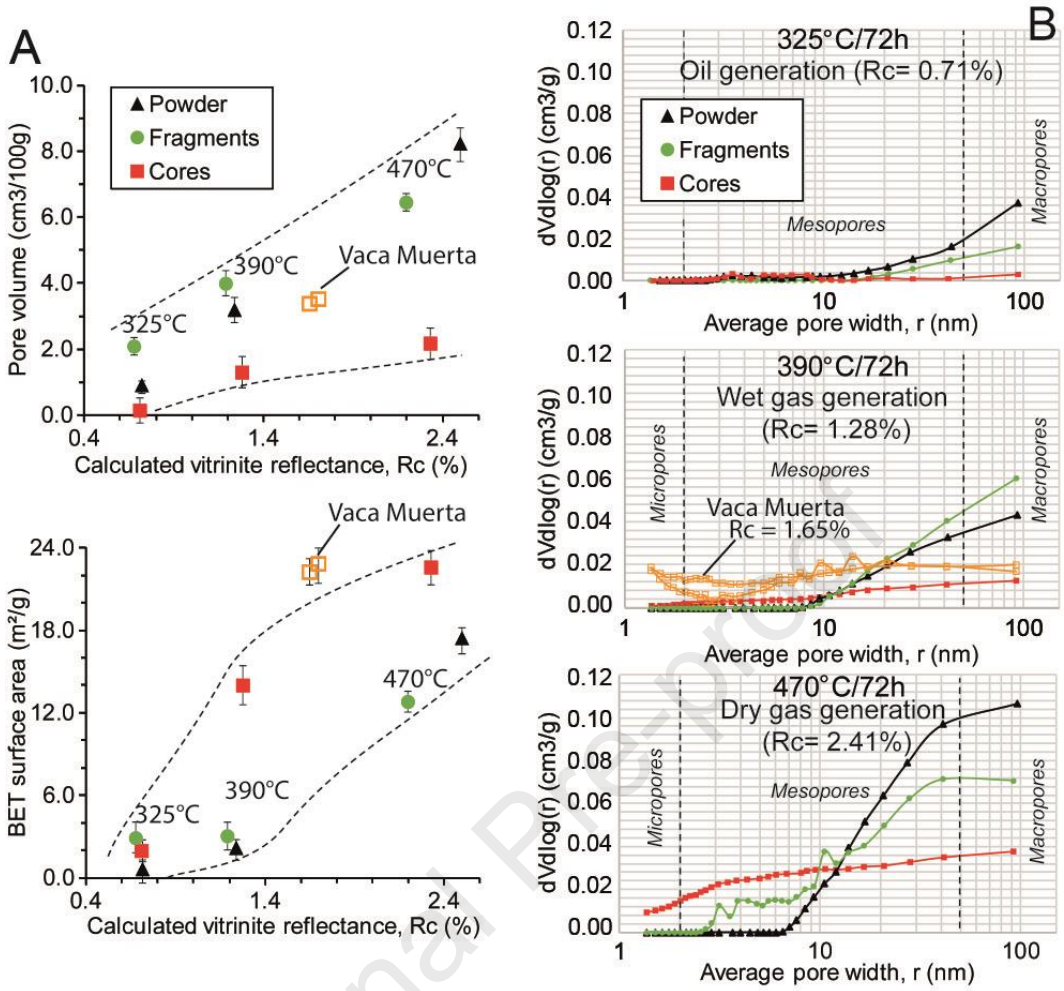

609

610 Fig.2. A) Pore volume, BET surface area, and B) BJH pore size distribution for the different rock fabric
611 after artificial maturation. B) displays the relative contribution to the total pore volume of pores over
612 any range of pore sizes. Comparison with Vaca Muerta samples (Cavelan et al., 2020b, 2019b). The
613 PSD curves presented in the figure are considered to be the most representative among the three
614 triplicates but PSD curves obtained for each triplicate are comparable (less than 10% of variation).

Declaration of interests

☒ The authors declare that they have no known competing financial interests or personal relationships that could have appeared to influence the work reported in this paper.

☐The authors declare the following financial interests/personal relationships which may be considered as potential competing interests: